



**HAL**  
open science

## **BAIN thin layers for deep UV applications**

Xin Li, Suresh Sundaram, Youssef El Gmili, Tarik Moudakir, Frédéric Genty,  
Sophie Bouchoule, Gilles Patriarche, Russell D. Dupuis, Paul L. Voss,  
Jean-Paul Salvestrini, et al.

► **To cite this version:**

Xin Li, Suresh Sundaram, Youssef El Gmili, Tarik Moudakir, Frédéric Genty, et al.. BAIN thin layers for deep UV applications. *physica status solidi (a)*, 2015, 212 (4), pp.745-750. 10.1002/pssa.201400199 . hal-01108100

**HAL Id: hal-01108100**

**<https://hal.science/hal-01108100>**

Submitted on 13 Jan 2022

**HAL** is a multi-disciplinary open access archive for the deposit and dissemination of scientific research documents, whether they are published or not. The documents may come from teaching and research institutions in France or abroad, or from public or private research centers.

L'archive ouverte pluridisciplinaire **HAL**, est destinée au dépôt et à la diffusion de documents scientifiques de niveau recherche, publiés ou non, émanant des établissements d'enseignement et de recherche français ou étrangers, des laboratoires publics ou privés.



Distributed under a Creative Commons Attribution - NonCommercial 4.0 International License

# BAlN thin layers for deep UV applications

Xin Li<sup>1,2</sup>, Suresh Sundaram<sup>2</sup>, Youssef El Gmili<sup>2</sup>, Tarik Moudakir<sup>2</sup>, Frédéric Genty<sup>3</sup>, Sophie Bouchoule<sup>4</sup>, Gilles Patriarche<sup>4</sup>, Russell D. Dupuis<sup>5</sup>, Paul L. Voss<sup>1,2</sup>, Jean-Paul Salvestrini<sup>2,6</sup>, and Abdallah Ougazzaden<sup>\*,1,2</sup>

<sup>1</sup> School of Electrical and Computer Engineering, Georgia Institute of Technology, GT-Lorraine, 57070 Metz, France

<sup>2</sup> UMI 2958, Georgia Tech-CNRS, 57070 Metz, France

<sup>3</sup> Supelec, LMOPS, EA 4423, 57070 Metz, France

<sup>4</sup> LPN CNRS, UPR20, 91460 Marcoussis, France

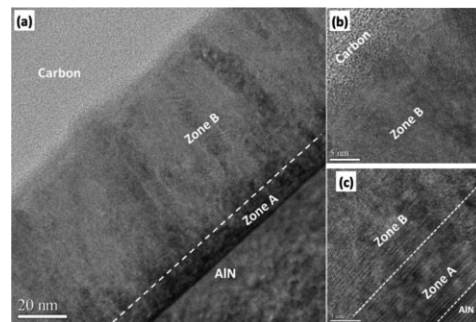
<sup>5</sup> Center for Compound Semiconductors and School of Electrical and Computer Engineering, Georgia Institute of Technology, Atlanta 30332, Georgia USA

<sup>6</sup> Université de Lorraine, LMOPS, EA 4423, 57070 Metz, France

**Keywords** III-nitrides semiconductors, BAlN, boron, MOVPE

In this work, wurtzite BAlN layers with boron composition as high as 12% were successfully grown by MOVPE. The growth was performed at 650 °C and then annealed at 1020 °C. Low temperature growth was used in order to alleviate *B*-rich phase poisoning under high TEB/III ratio. The growth was performed by continuous epitaxy as well as by flow-modulate epitaxy. BAlN single layers with clearly defined X-ray diffraction peaks were achieved on AlN templates which are appropriate substrates for deep UV devices, as well as on GaN templates to facilitate distinguishing of the XRD peak of BAlN from the substrate peak. The layer demonstrated columnar crystalline features and inherited wurtzite structure from substrates.

Cross-section STEM image (bright field) of 75 nm thick BAlN layers containing 12% boron taken along the [11-2 0] zone axis. Zone A is lattice-oriented along *c*-axis and zone B has columnar structure; (b) higher magnification image for the top part of the layer; (c) higher magnification image for the film/substrate interface.



**1 Introduction** III-nitrides are wide band gap semiconductors for a variety of electronic and optoelectronic devices. In the last two decades, many efforts have been devoted to AlInGaN materials, which have led to remarkable progress of light emitting devices in visible and UV spectra region. Compared with conventional AlInGaN system, boron containing III-nitrides are quite new in this family. They are suitable for deep UV applications because of wide band gap. At the same time, the BAlGaN system can decrease or eliminate lattice

mismatch on SiC and AlN substrates [1–4]. Additionally, it has been found that only a small amount of boron incorporation in AlN can introduce a strong refractive index contrast. This is of great interests for high reflectivity III-N DBRs in the deep UV region [5, 6]. Boron containing III-nitrides can bring additional freedom in engineering the bandgap, lattice constant, and refractive index of multi-structure devices; however, further investigation of the basic epitaxial growth is required for this new material. BAlN and B GaN have been grown by MOVPE [3, 5–13],

MBE [4, 14, 15], and magnetron sputtering [16, 17], but the boron content and crystallinity are limited due to phase separation, short diffusion length of boron, and strong parasitic reaction in the gas phase [3, 10, 14, 16]. In order to enhance migration of boron and aluminum atoms for MOVPE, BAIN materials have normally been grown above 1050 °C [3, 5, 7, 18], or at 1000 °C by using flow-modulate epitaxy (FME) [10, 19]. However, for the MOVPE growth, clear XRD peaks of w-BAIN layers relating to only 1–2% boron have been reported [3, 5, 10, 18]. High boron content was also demonstrated [7] but the related XRD peak intensity was very weak. The drawback by using high temperature for incorporating more boron in single layer is that B-rich phase would poison the growth under high TEB/III ratio [20].

In this paper, in order to obtain BAIN with high boron content, BAIN films have been grown at 650 °C and then annealed at 1020 °C. The influence of growth temperature was investigated and it shows that the crystallinity of BAIN grown under high TEB/III ratio was deteriorated by increasing temperature above 650 °C. By continuous growth, from 1.2% to 5.6% boron was obtained by varying TEB/III ratio. Flow-modulate epitaxy was also applied and BAIN containing as high as 12% boron was successfully achieved on both AlN and GaN templates. Single solid phase BAIN was clearly identified by high-resolution XRD. TEM characterizations show that the BAIN layer consists of columnar polycrystals, and it inherits the wurzite structure of the substrate.

**2 Experimental procedures** BAIN layers were grown in a MOVPE T-shape reactor [21] at 100 Torr by using hydrogen as carrier gas. The growth was performed on two types of substrates: 1 μm AlN templates on sapphire and 3 μm GaN templates on sapphire. As shown in Fig. 1, the substrates were annealed in hydrogen at 1040 °C prior to growth. Thin BAIN layers were grown at low temperature, which was varied from 650 to 800 °C to study its influence. Then the temperature was ramped up to 1020 °C and the samples were annealed for 5 min before cooling down.

A large flow rate of NH<sub>3</sub> (2.3 slm/min) was used due to inefficient decomposition of NH<sub>3</sub> at low temperature. In order to investigate boron incorporation, the flow-rate of

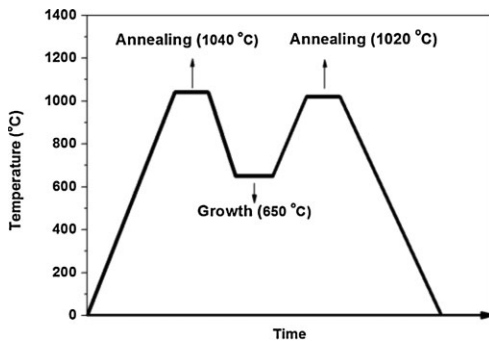


**Figure 1** Schematic of growth procedure.

TMAI was maintained constant, while flow rate of TEB was varied to have TEB/III molar ratio in the vapor phase of 0, 9, 17, and 39%, respectively. For flow-modulate epitaxy (FME), the feeding sequences of precursors during the growth was shown in Fig. 2: 2 s supply of metalorganics and 1 s supply of NH<sub>3</sub> were alternatively run into the reactor without interruption [10].

High-resolution X-ray diffraction (XRD) measurements were performed in a Panalytical X'pert Pro MRD system with Cu Kα radiation. The crystallinity of BAIN layers were evaluated by  $2\theta-\omega$  scans. The boron composition was estimated by *c*-lattice parameters assuming Vegard's law of the alloys. The depth concentration profiles for Al, B, N, were performed by secondary ion mass spectroscopy (SIMS) analysis.

The growth rate of the layers was determined from interference fringes of *in situ* reflectance for thick layer growth, and thickness of thin layers can be calculated by growth time. Surface morphology was characterized by atomic force microscope (AFM). The sample was then prepared for scanning transmission microscopy (STEM) using focused ion beam (FIB) thinning and ion milling. One-hundred nanometer carbon was deposited before FIB in order to protect the surface. High-angle annular dark-field scanning transmission microscopy (HAADF-STEM) characterizations were performed on aberration-corrected JEOL 2200FS electron transmission microscope.

### 3 Results and discussion

**3.1 Influence of growth temperature** The growth was performed on GaN templates under high TEB/III ratio 39%. As shown in Fig. 3a, BAIN single layer grown at 650 °C with 20 nm thickness demonstrates an X-ray diffraction peak at 36.38° (± 0.17°), which indicates that the layer has smaller lattice constant *c* than AlN due to boron substituting Al atoms in the crystal structure. We can assume the layer is fully-relaxed considering the large lattice mismatch between BAIN layer and GaN template. In this case, the *c*-lattice constant is 4.935 Å (± 0.022 Å), which corresponds to boron composition of 5.6% (± 2.8%) by applying Vegard's law. The complete relaxation of the layer can be confirmed in Fig. 4: when we stop TEB flow

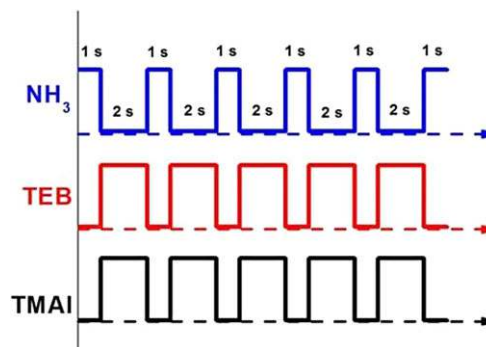


**Figure 2** Feeding sequences of precursors for flow-modulate epitaxy method.

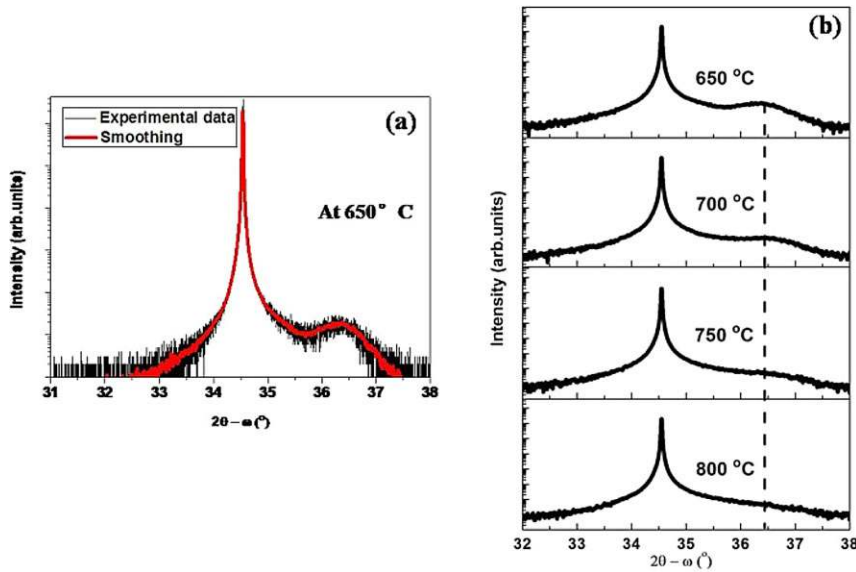


**Figure 3** (a) HR-XRD  $2\theta-\omega$  scan of 20 nm BAIN layers grown on GaN template at 650 °C under TEB/III = 39%; (b) shows the influence of growth temperature which was varied between 650 and 800 °C.

and only grow AlN layer, the  $2\theta-\omega$  peak of the layer is located at 36.02° corresponding to completed relaxed AlN layer.

When the deposition temperature is increased, shown in Fig. 3b, the BAIN peak is weakened, and then disappears when it is increased to 800 °C. It indicates that under this

high TEB/III ratio the crystallinity is worse when the layer is grown at higher temperature. So the following results in this paper are all referred to the growth at 650 °C.

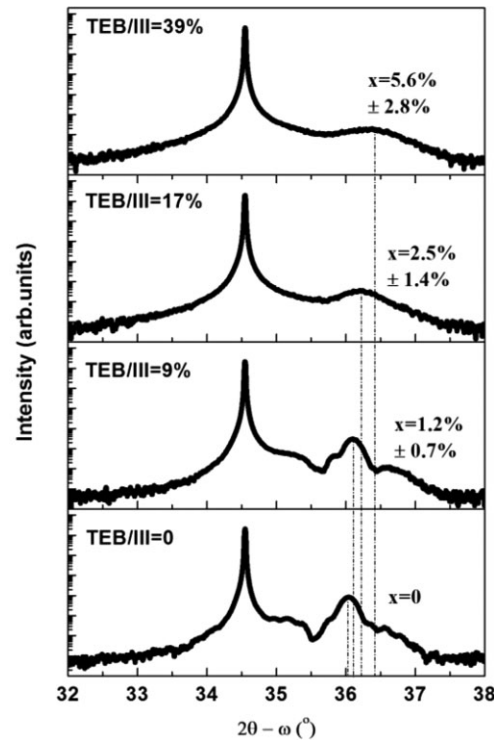


**Figure 4** HR-XRD  $2\theta-\omega$  scans of 20 nm BAIN grown on GaN templates by continuous method under different TEB/III ratio.

**3.2 Influence of TEB/III ratio** In order to have different amount of boron incorporation, a series of samples were grown on GaN templates by continuous method, and TEB/III ratio was changed run to run. As shown in Fig. 4, when TEB/III ratio is increased from 0 to 39%, the peak of the layer shifts gradually towards greater diffraction angles (0–5.6% boron). The peak is broadened with fringes missing due to the polycrystalline nature of BAIN, which would be discussed later. Figure 5 shows that boron content in solid phase has almost a linear relationship with TEB/III ratio in the gas phase.

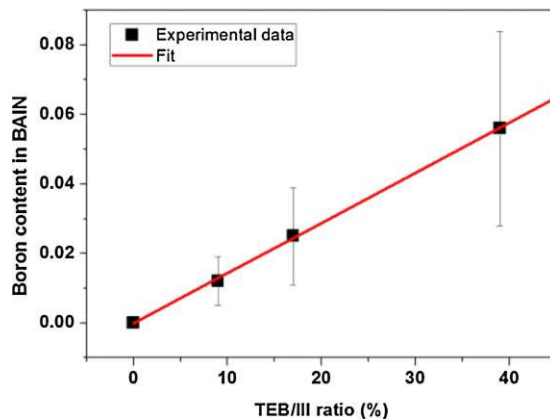


**Figure 5** Relationship between boron content in solid phase and TEB/III ratio in gas phase for 20 nm BAIN layers grown on GaN templates by continuous growth.

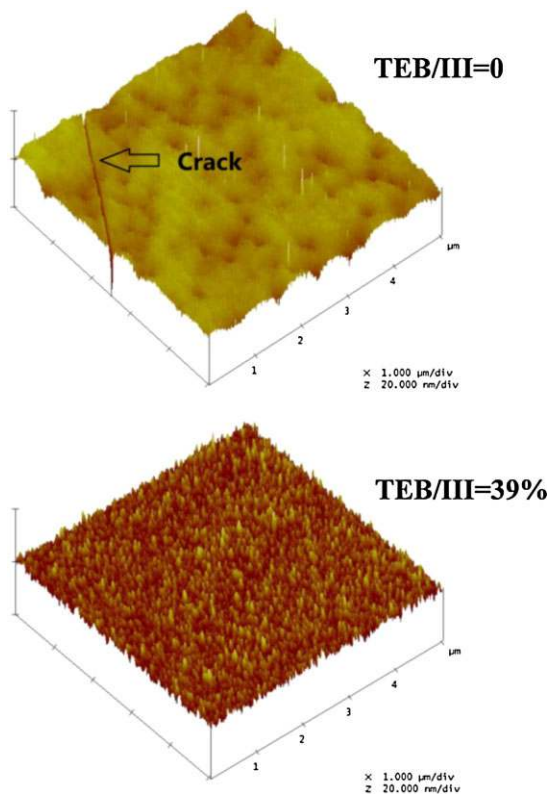


**Figure 6** AFM images of 40 nm BAIN layers grown on GaN templates under TEB/III ratio of 0 and 39%.

The morphology change was studied by AFM in Fig. 6. As we can see, without boron incorporation, 40 nm AlN layer on GaN template exhibits normal V-defects and cracks generated by lattice mismatch. The flat area between defects has surface roughness around 0.7 nm. When boron was incorporated, the surface became rough, and cracks and V-defects disappeared. The surface was covered by small crystallites caused by columnar growth of BAIN, and this columnar feature would be clearly observed by STEM results in the following section. Surface roughness was around 1.2 nm for TEB/III = 39% (~5.6% boron in solid phase).

**3.3 BAIN growth by FME** For BAIN layers grown on AlN templates by continuous flow, the XRD peak of BAIN layer was too weak and it cannot be distinguished from noise. So we applied FME method to improve the crystalline quality. The feeding sequences are shown in Fig. 2, and 75 nm BAIN layer was grown under TEB/III = 39%. As shown in Fig. 7, clear XRD peaks can be identified at  $36.59^\circ (\pm 0.20^\circ)$  on both GaN and AlN templates. Lattice constant  $c$  is  $4.908 \text{ \AA} (\pm 0.025 \text{ \AA})$  and the corresponding boron content is 9% ( $\pm 3.2\%$ ). Since BAIN peak is very close to AlN template peak, the deconvolution of substrate peak and layer peak is shown in the inset figure.

The concentration calculated by XRD has a large error range because of the broadness of the BAIN diffraction peak and uncertainty of the lattice parameters and strain. These all

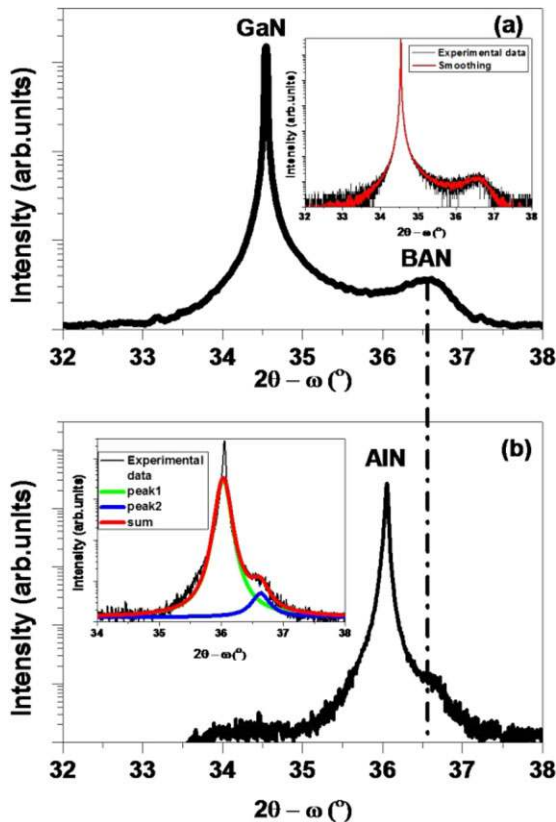


**Figure 7** HR-XRD of 70 nm BAIN on: (a) GaN template; and (b) AlN template by FME growth (TEB/III = 39%). Inset figures show the smoothing and deconvolution of two peaks.

influence calculation of the composition from diffraction peak positions, especially for the layer with high boron content. So the boron incorporation into the layer was also analyzed by SIMS profile along the growth direction in Fig. 8. The Al signal is decreased in the BAIN layer

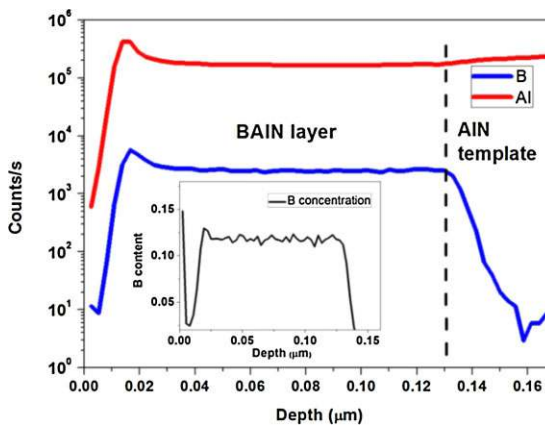


**Figure 8** SIMS elemental concentration depth profiles of B and Al for the sample grown on AlN template; the inset shows the boron concentration obtained by using boron implanted AlN as calibration sample.

compared with the signal of the template indicating that boron atoms were substitutionally incorporated into AlN lattice. Boron has a uniform distribution along the growth direction. The concentration of boron can be calculated based on atomic concentration obtained by SIMS. In order to calibrate the SIMS signal for quantitative measurements, a boron-implanted AlN sample with known boron content was used as a reference. The concentration of boron calculated from the SIMS signal is 12% with 0.6% error (inset of Fig. 8), which agrees with the composition range given by XRD diffraction peak positions (6–12%).

Compared with the continuous growth under same TEB/III ratio in Fig. 4, more boron was incorporated by FME method, and the possible reason could be that parasitic reaction in the gas phase can be eliminated by pulsing precursors. The successful growth of BAlN on AlN templates gives immense potential for deep-UV applications.

STEM characterizations were also performed to study the crystallinity of the layer. The cross-section image in Fig. 9

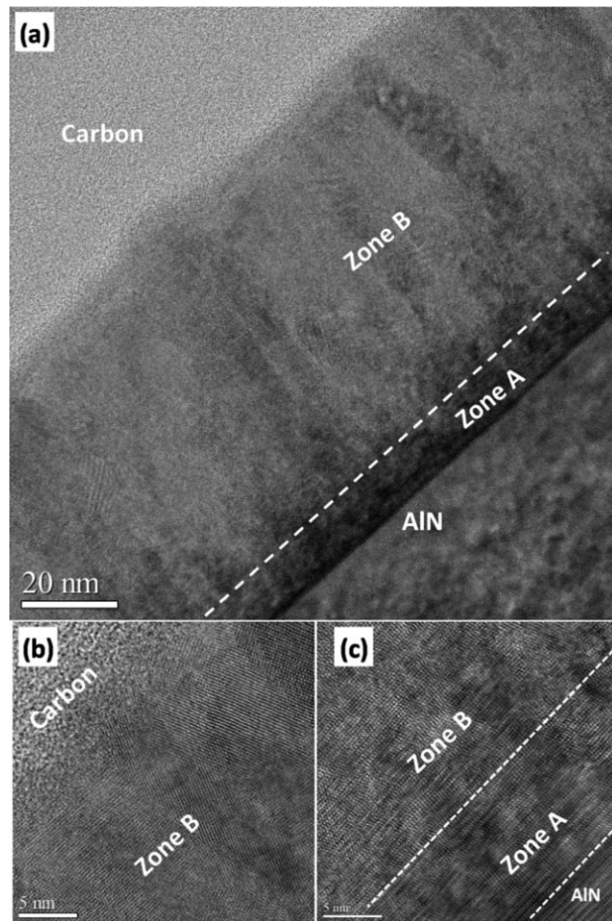


**Figure 9** (a) Cross-section STEM image (bright field) of 75 nm thick BAlN layers containing 12% boron taken along the  $[1\ 1\ -2\ 0]$  zone axis. Zone A is lattice-oriented along  $c$ -axis and Zone B has columnar structure; (b) higher magnification image for the top part of the layer; (c) higher magnification image for the film/substrate interface.

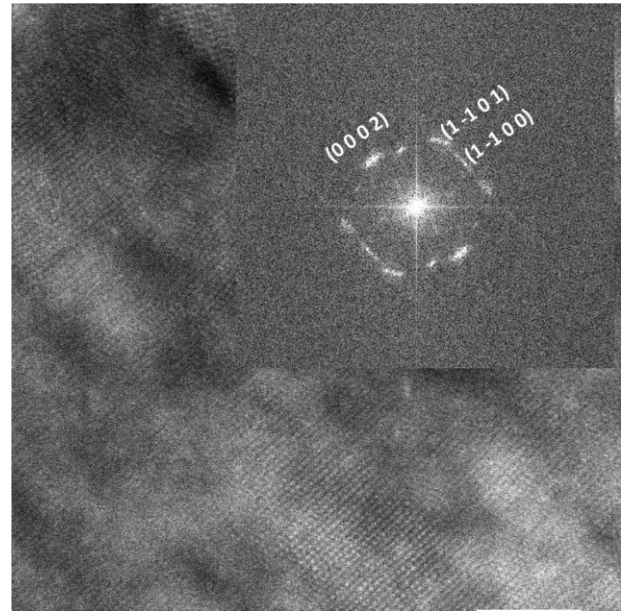


**Figure 10** Cross-section high-angle annular dark field scanning transmission microscopy (HAADF-STEM) image of 75 nm BAlN layer containing 12% boron; the inset shows diffraction pattern after fast Fourier transform (FFT).

shows that BAlN layer has a columnar crystalline growth feature. At the beginning of BAlN growth, the lattice is still oriented along  $c$ -axis (the zone A). After around 10 nm, the crystals start to disorient and form columns (zone B). The lattice of columnar crystals can be clearly observed in Fig. 9b which is the top part of the layer. This columnar growth feature would lead to surface roughness, as observed in AFM analysis.

Figure 10 presents high-angle annular dark-field scanning transmission microscopy (HAADF-STEM) image of the BAlN layer and diffraction pattern after Fast Fourier Transform (FFT). It exhibits mainly the typical pattern of the wurtzite crystal along the  $[11\bar{2}0]$  zone axis, even though the diffraction spots are elongated due to the different tilts of columnar polycrystals.

**4 Conclusion** In summary, we demonstrated low temperature MOVPE growth of BAlN alloys with high boron incorporation. It is found that low temperature has alleviated boron poisoning issue during growth under high TEB/III ratio. Wurtzite BAlN layers with boron as high as 12% were obtained on both GaN and AlN templates. The promising results advance prospects for MOVPE-grown boron alloys, which can result in more freedom in bandgap, strain engineering with tailoring of refractive index of DBR structures for eventual deep-UV sources.

**Acknowledgments** The authors would like to thank David Troadec from IEMN in Lille for FIB preparation. The work was supported by French ANR (Agence Nationale de la Recherche) in the framework of VESUVE project (ANR-11-BS03-0012).

## References

- [1] Y. Kuga, T. Shirai, M. Haruyama, H. Kawanishi, and Y. Suematsu, *J. Appl. Phys.* **34**, 4085 (1995).
- [2] M. Haruyama, T. Shirai, H. Kurimoto, and H. Kawanishi, *Proc. Int. Symp. on Blue Laser and Light Emitting Diode*, Tokyo, p. 106 (1996).
- [3] A. Y. Polyakov, M. Shin, W. Qian, M. Skowronski, D. W. Greve, and R. G. Wilson, *J. Appl. Phys.* **81**, 1715 (1997).
- [4] A. Nakajima, Y. Furukawa, H. Yokoya, and H. Yonezu, *J. Cryst. Growth* **278**, 437 (2005).
- [5] S. Watanabe, T. Takano, K. Jinen, J. Yamamoto, and H. Kawanishi, *Phys. Status Solidi C* **0**(7), 2691 (2003).
- [6] M. Abid, T. Moudakir, G. Orsal, S. Gautier, A. E. Naciri, Z. Djebbour, J.-H. Ryou, G. Patriarche, L. Largeau, H. J. Kim, Z. Lochner, K. Pantzas, D. Alamarguy, F. Jomard, R. D. Dupuis, J.-P. Salvestrini, P. L. Voss, and A. Ougazzaden, *Appl. Phys. Lett.* **100**, 051101 (2012).
- [7] M. Shibata, M. Kurimoto, J. Yamamoto, T. Honda, and H. Kawanishi, *J. Cryst. Growth* **189–190**, 445 (1998).
- [8] C. H. Wei, Z. Y. Xie, J. H. Edgar, K. C. Zeng, J. Y. Lin, H. X. Jiang, J. Chaudhuri, C. Ignatiev, and D. N. Braski, *J. Electron. Mater.* **29**, 452 (2000).
- [9] T. Takano, M. Kurimoto, J. Yamamoto, and H. Kawanishi, *J. Cryst. Growth* **237–239**, 972 (2002).
- [10] T. Akasaka and T. Makimoto, *Appl. Phys. Lett.* **88**, 041902 (2006).
- [11] S. Gautier, C. Sartel, S. O. S. Hamady, N. Maloufi, J. Martin, F. Jomard, and A. Ougazzaden, *Superlattices Microstruct.* **40**, 233 (2006).
- [12] G. Orsal, N. Maloufi, S. Gautier, M. Alnot, A. A. Sirenko, M. Bouchaour, and A. Ougazzaden, *J. Cryst. Growth* **310**, 5058 (2008).
- [13] A. Ougazzaden, S. Gautier, T. Moudakir, Z. Djebbour, Z. Lochner, S. Choi, H. J. Kim, J.-H. Ryou, R. D. Dupuis, and A. A. Sirenko, *Appl. Phys. Lett.* **93**, 083118 (2008).
- [14] J. H. Edgar, D. T. Smith, C. R. Eddy, C. A. Carosella, and B. D. Sartwell, *Thin Solid Films* **298**, 33 (1997).
- [15] V. K. Gupta, C. C. Wamsley, M. W. Koch, and G. W. Wicks, *J. Vacuum Sci. Technol. B* **17**, 1246 (1999).
- [16] L. Liljeholm and J. Olsson, *Vacuum* **86**, 466 (2011).
- [17] J.-H. Song, J.-L. Huang, J. C. Sung, S.-C. Wang, H.-H. Lu, and D.-F. Lii, *Thin Solid Films* **519**, 4212 (2011).
- [18] H. Kawanishi and T. Honda, *Photonics Based on Wavelength Integration and Manipulation*, IPAP Books 2, 19 (2005).
- [19] T. Akasaka, Y. Kobayashi, and T. Makimoto, *Appl. Phys. Lett.* **91**, 041914 (2007).
- [20] A. Y. Polyakov, M. Shin, M. Skowronski, D. W. Greve, R. G. Wilson, A. V. Govorkov, and R. M. Desrosiers, *J. Electron. Mater.* **26**, 237 (1997).
- [21] S. Gautier, C. Sartel, S. Ould-Saad, J. Martin, A. Sirenko, and A. Ougazzaden, *J. Cryst. Growth* **298**, 428 (2007).